Research Square

Preprints are preliminary reports that have not undergone peer review.
They should not be considered conclusive, used to inform clinical practice,
or referenced by the media as validated information.

Intestinal Toxicity Profile of PD-1 Inhibitor Combined with Platinum-Based Chemotherapy in a Lewis Lung Carcinoma Mouse Model

Fan-Lei Kong

Kongfanlei_md@126.com

Qilu Hospital of Shandong University

li dai

Shandong Provincial Hospital

Article

Keywords: PD-1 inhibitor, platinum-based chemotherapy, intestinal microenvironment, gastrointestinal toxicity, isobutyrate, Lewis lung carcinoma

Posted Date: November 13th, 2026

DOI: https://doi.org/10.21203/rs.3.rs-11093020/v1

License: This work is licensed under a Creative Commons Attribution 4.0 International License.
Read Full License

Additional Declarations: No competing interests reported.

Intestinal Toxicity Profile of PD-1 Inhibitor Combined with Platinum-Based Chemotherapy in a Lewis Lung Carcinoma Mouse Model

Li Dai[1], Fan-lei Kong[2]

1. Department of Stomatology, Shandong Provincial Hospital, Jinan, China

2. Department of Radiology, Qilu Hospital of Shandong University, Jinan, China

* Correspondence:

Fan-Lei Kong, M.D., Department of Radiology, Qilu Hospital of Shandong University, Jinan, 250000，China

E-mail: Kongfanlei_md@126.com

Telephone: +86 18518052427

Word count: 4774

Number of figures: 6

Running title: PD-1 inhibitor and chemotherapy differentially perturb intestinal microenvironment

Keywords: PD-1 inhibitor; platinum-based chemotherapy; intestinal microenvironment; gastrointestinal toxicity; isobutyrate; Lewis lung carcinoma

Author contributions: Kong FL designed the research and contributed to the review and editing of the manuscript; Li Dai performed the research, analyzed the data and wrote the paper.

Funding: Supported by Natural Science Foundation of Shandong Province (ZR2023QH485 and ZR2023QH328)

Ethical statement: This study was approved by The Animal Care and Use committee of Qilu Hospital of Shandong University（No.KYLL-2022(ZM)-1121）

Conflict-of-interest statement: The authors declare that they do not have any affiliation with or financial relationship/interest in a commercial organization that could pose a conflict of interest.

Abstract

PD-1 inhibitor combined with platinum-based chemotherapy is the standard first-line treatment for advanced non-small cell lung cancer, but whether this combination exacerbates gastrointestinal toxicity remains unclear. In this descriptive study, we characterized the intestinal toxicity profile of PD-1 inhibitor and chemotherapy, alone and in combination, in a Lewis lung carcinoma mouse model. C57BL/6J mice bearing Lewis lung tumors were randomized into five groups (n = 8 per group): Control, Model, chemotherapy (carboplatin/pemetrexed), immunotherapy (anti-PD-1), and combination. Gastrointestinal toxicity was assessed by body weight, food and water intake, serum albumin and prealbumin, diarrhea score, disease activity index, colon length, and histopathological scoring. Intestinal barrier gene expression, mucosal immune parameters, inflammatory cytokine expression, and fecal short-chain fatty acids were measured. Combination therapy achieved superior antitumor efficacy compared with monotherapy ($p < 0.05$). Gastrointestinal toxicity in the combination group was comparable to chemotherapy alone ($p > 0.05$) but higher than in the Model and anti-PD-1 groups ($p < 0.01$). Chemotherapy was associated with reduced colonic occludin and claudin-1 mRNA expression ($p < 0.05$), and the addition of PD-1 inhibitor did not further alter this parameter. Foxp3 mRNA was lower in anti-PD-1-containing groups ($p < 0.05$). The anti-PD-1 group

showed elevated colonic IFN-γ and reduced IL-10 mRNA ($p < 0.05$), with parallel changes in tumor tissues. Among short-chain fatty acids, isobutyrate was elevated in anti-PD-1-treated mice ($p < 0.05$), whereas other short-chain fatty acids showed no significant differences. These observations describe the differential intestinal toxicity profiles associated with chemotherapy and PD-1 inhibitor treatment and suggest associations that warrant further investigation.

Keywords: PD-1 inhibitor; platinum-based chemotherapy; intestinal microenvironment; gastrointestinal toxicity; isobutyrate; Lewis lung carcinoma

Introduction

c Immune checkpoint inhibitors (ICIs), particularly antibodies targeting programmed cell death protein-1 (PD-1) and its ligand PD-L1, have revolutionized the treatment landscape for advanced non-small cell lung cancer (NSCLC) [1,2]. The combination of PD-1 inhibitors with platinum-based doublet chemotherapy is now the standard first-line therapy for NSCLC patients without targetable genetic alterations, demonstrating superior survival outcomes compared with chemotherapy alone [3,4].

Despite these clinical advances, immune-related adverse events (irAEs) remain a significant challenge. Among these, gastrointestinal (GI) toxicity—manifesting as diarrhea, colitis, and in severe cases, intestinal perforation—is one of the most common and clinically consequential irAEs, often leading to treatment interruption or discontinuation [5,6]. The incidence of diarrhea ranges from approximately 13% with PD-1 inhibitor monotherapy to 20–21% when combined with platinum-based chemotherapy [7–9].

The intestinal microenvironment comprises multiple interacting components: the physical barrier

(epithelial tight junctions), mucosal immunity (IgA, T cells, regulatory T cells [Tregs]), inflammatory mediators (cytokines), and microbial metabolites (short-chain fatty acids [SCFAs]) [10,11]. Both chemotherapy and ICIs have been reported to affect these components, albeit potentially through distinct mechanisms. Chemotherapy-induced diarrhea (CID) is primarily attributed to direct cytotoxicity to intestinal epithelial cells, leading to mucosal barrier disruption through tight junction protein downregulation [12,13]. In contrast, ICI-related colitis is thought to result from immune dysregulation, characterized by hyperactivation of effector T cells and impairment of Treg function [14,15].

A critical but unresolved question is whether the combination of PD-1 inhibitors and platinum-based chemotherapy results in synergistic or additive GI toxicity. Given that these two therapeutic modalities may affect different components of the intestinal microenvironment, it is plausible that their concurrent administration does not necessarily amplify GI adverse effects. However, systematic preclinical evaluation of this hypothesis is lacking.

The gut microbiota and its metabolites, particularly SCFAs, play essential roles in maintaining intestinal immune homeostasis. SCFAs such as butyrate promote Treg differentiation and enhance epithelial barrier function [16,17]. We have previously characterized the alterations in gut microbiota composition in this LLC mouse model treated with PD-1 inhibitor and chemotherapy using 16S rRNA gene sequencing [18]. However, the accompanying changes in SCFA profiles and their relationship with GI toxicity and mucosal immune parameters remain to be elucidated.

In this study, we used an LLC mouse model to descriptively characterize the intestinal toxicity profile of PD-1 inhibitor combined with platinum-based chemotherapy. We assessed physical barrier gene expression, mucosal immune parameters, inflammatory cytokine expression, and microbial

metabolites (SCFAs). Building on our previously published microbiota compositional data, we now investigate whether the functional metabolic output of the microbiota is altered by combination therapy. We aimed to determine whether combination therapy causes synergistic GI toxicity and to describe the associated changes in the intestinal microenvironment.

Materials and Methods

Animals and Tumor Model

Male C57BL/6J mice (6--8 weeks old, 20--22 g) were purchased from Beijing Vitong Lihua Biotechnology Co., Ltd. and housed under specific pathogen-free (SPF) conditions (12 h light/dark cycle, 22 ± 1°C, 60--70% humidity) with standard chow and water ad libitum. All animal experiments were approved by the Ethics Committee of Qilu Hospital, Shandong University [KYLL-2022(ZM)-1211]. All methods were performed in accordance with the relevant guidelines and regulations, and all animal procedures complied with the ARRIVE guidelines 2.0 and the American Veterinary Medical Association (AVMA) Guidelines for the Euthanasia of Animals.

Lewis lung carcinoma cells were obtained from the Chinese Academy of Sciences Cell Bank (Resource No. 3101MOUTCM7). The direct link to the cell line information is as follows: https://www.cellbank.org.cn/search-detail.php?id=78. LLC cells were cultured in RPMI-1640 medium supplemented with 10% fetal bovine serum at 37°C in a humidified atmosphere with 5% CO_2. Cells in the logarithmic growth phase were harvested, resuspended in phosphate-buffered saline (PBS) at a concentration of 1×10^7 cells/mL. Mice were subcutaneously inoculated with 0.2 mL of cell suspension into the right forelimb axilla.

Experimental Design and Treatment

Twelve days after tumor inoculation (D12), mice with well-formed tumors (volume 50--100 mm^3)

were randomized into four groups (n = 8/group): Model (saline), CARB/PEM (chemotherapy), aPD-1 (immunotherapy), and CARB/PEM/aPD-1 (combination therapy). An additional group of eight non-tumor-bearing mice served as the Control group. The treatment period comprised two 7-day cycles (14 days total), and all mice were sacrificed on D26 by isoflurane overdose followed by cervical dislocation. Mice were included if tumor volume 50–100 mm^3, regular shape, body weight 20–28 g, normal activity on D12. Excluded if tumor outside range, ulcerated/necrotic, >15% weight loss, or signs of severe illness. On D12, eligible tumor-bearing mice were randomly assigned to four groups (Model, CARB/PEM, aPD-1, Combination) using a random number table generated by Microsoft Excel (RAND function). Each mouse was assigned a unique identifier, a random number was generated, and mice were sorted by their random numbers for sequential group allocation. The Control group (non-tumor-bearing) was not subjected to randomisation.

Treatment regimens were as follows:

- Control group: intraperitoneal (i.p.) saline, same schedule as combination group.
- Model group: i.p. saline, same schedule as combination group.
- CARB/PEM group: carboplatin 60.8 mg/kg + pemetrexed 112.45 mg/kg, i.p., on D12 and D19.
- aPD-1 group: anti-mouse PD-1 antibody (200 μg/mouse, i.p.) on D12, D15, D19, and D22.
- Combination group: CARB/PEM on D12 and D19 + aPD-1 on D12, D15, D19, and D22, at the same doses as above.

Euthanasia and Sample Collection

At the experimental endpoint (D26), all mice were euthanized by isoflurane inhalation overdose (5% isoflurane in 100% oxygen, delivered via a precision vaporizer at a flow rate of 1–2 L/min) in an

induction chamber until loss of righting reflex and cessation of respiration (approximately 3–5 min). Death was confirmed by absence of corneal reflex and cessation of heartbeat. Cervical dislocation was subsequently performed as a secondary physical method to ensure death, in accordance with AVMA guidelines. All efforts were made to minimize animal suffering throughout the experimental period.

Whole blood was immediately collected by cardiac puncture post-euthanasia and centrifuged (3,000 rpm, 5 min, 4°C). Serum was aliquoted and stored at -80°C. The spleen was dissected and weighed, and the spleen index was calculated as spleen weight (mg) / body weight (g) × 10. The colon was excised from the cecocolonic junction to the anus, and its length was measured. A 2-cm segment of the distal colon was fixed in 4% paraformaldehyde for histopathological analysis. The remaining colon tissue was snap-frozen in liquid nitrogen and stored at -80°C for RNA extraction and ELISA. Fecal samples were collected from the colon and stored at -80°C for SCFA analysis. Tumor tissues were excised, measured, photographed, and snap-frozen for ELISA.

Assessment of General Condition and GI Toxicity

Body weight and tumor volume were measured every 2 days. Tumor volume (V) was calculated as $V = a \times b^2/2$, where a is the longest diameter and b is the perpendicular diameter. Food and water intake were monitored every 2 days by weighing the remaining chow and water in each cage.

Disease activity index (DAI) was assessed every 2 days based on a composite score incorporating weight loss, stool consistency, and fecal blood (Table 1). Diarrhea severity was scored every 2 days using a 0--3 scale: 0, normal pellets; 1, slightly moist or soft stool; 2, moderately wet, unformed stool; 3, watery stool.

At sacrifice (D26), whole blood was collected and centrifuged (3000 rpm, 5 min). Serum albumin

(ALB) and prealbumin (PA) levels were measured using an automatic biochemical analyzer. The spleen was dissected and weighed, and the spleen index was calculated as spleen weight (mg) / body weight (g) × 10. The colon was excised from the cecocolonic junction to the anus, and its length was measured.

Histopathological Analysis

A 2-cm segment of the distal colon was fixed in 4% paraformaldehyde, embedded in paraffin, sectioned at 4 μm thickness, and stained with hematoxylin-eosin (HE). Histopathological changes, including inflammatory cell infiltration, crypt architecture disruption, epithelial damage, and edema, were evaluated and scored by an experienced pathologist blinded to group allocation.

Quantitative Real-Time PCR (RT-qPCR)

Total RNA was extracted from colon tissues using TRIzol reagent. RNA concentration and purity were determined using a Nanodrop 2000 spectrophotometer. Complementary DNA (cDNA) was synthesized using a reverse transcription kit (Servicebio). qPCR was performed using 2× qPCR Mix with gene-specific primers. The primer sequences are listed in Table 3. Relative mRNA expression was calculated using the 2^(-ΔΔCt) method with GAPDH as the internal reference.

Target genes: Occludin, Claudin-1, Foxp3, IL-10, IFN-γ.

Immunofluorescence for IgA+ Cells

Paraffin-embedded colon sections were deparaffinized, rehydrated, and subjected to antigen retrieval. After blocking, sections were incubated with primary antibody (Anti-IgA) at 4°C overnight. The following secondary antibodies (Servicebio) were used as appropriate: Cy3-conjugated goat anti-rabbit (GB21303, 1:300), HRP-conjugated rabbit anti-goat (GB23204, 1:500), Cy3-conjugated goat anti-mouse (GB21301, 1:300), among others (see Supplementary Table S1 for

complete list). Nuclei were counterstained with DAPI. IgA+ cells were quantified using Aipathwell software, and the positive cell ratio was calculated as IgA+ cells / total cells.

Enzyme-Linked Immunosorbent Assay (ELISA)

Colonic mucosal SIgA was extracted by scraping the mucosal surface, homogenizing in PBS, and centrifuging. SIgA concentration in the supernatant was measured using a Mouse SIgA ELISA Kit. Colonic IL-17 and TGF-β levels were measured using commercial ELISA kits. Tumor tissue homogenates were prepared, and IL-10 and IFN-γ levels were measured by ELISA. All procedures were performed according to the manufacturers' instructions.

Targeted Short-Chain Fatty Acid (SCFA) Quantification

Fecal samples collected at the end of treatment (D26) were analyzed for SCFA content (acetate, propionate, butyrate, isobutyrate, valerate, isovalerate, hexanoate) using liquid chromatography-tandem mass spectrometry (LC-MS/MS). Briefly, fecal samples (50 ± 2 mg) were homogenized in 500 μL of deionized water, acidified with 50 μL of 50% sulfuric acid, and extracted with 1 mL of diethyl ether. After centrifugation (12,000 rpm, 10 min, 4°C), the organic phase was collected and analyzed on an Agilent 6460 LC-MS/MS system equipped with an ACQUITY UPLC HSS T3 column (2.1 × 100 mm, 1.8 μm). The mobile phase consisted of 0.1% formic acid in water (A) and acetonitrile (B) at a flow rate of 0.3 mL/min. SCFA concentrations were quantified against standard calibration curves using internal standard (2-ethylbutyric acid).

Gut Microbiota Analysis

The 16S rRNA gene sequencing and bioinformatics analysis of the gut microbiota in this animal model have been previously published [18]. Relevant findings are cited and briefly discussed in context.

Statistical Analysis

All data are expressed as mean ± standard deviation (SD). Statistical analyses were performed using SPSS 16.0. Comparisons among multiple groups were performed by one-way analysis of variance (ANOVA) followed by appropriate post-hoc tests. For data with non-normal distribution (e.g., SCFAs), Kruskal-Wallis test followed by Dunn's post-hoc test was applied. A p-value < 0.05 was considered statistically significant. Graphs were generated using GraphPad Prism software.

Results

3.1 Combination therapy achieves superior antitumor efficacy

Before treatment initiation, tumor volumes did not differ among the Model, chemotherapy, anti-PD-1, and combination groups ($p > 0.05$). After two treatment cycles, tumor volumes in all three treatment groups were smaller than those in the Model group (chemotherapy: $p < 0.05$; anti-PD-1: $p < 0.05$; combination: $p < 0.01$; Fig. 1A, B). The combination group showed the most pronounced tumor inhibition, with final tumor volumes smaller than those in both monotherapy groups (both $p < 0.05$; Fig. 1C, D).

3.2 Gastrointestinal toxicity profile

To evaluate GI toxicity, we assessed body weight, food/water intake, nutritional indices, spleen index, diarrhea, DAI, colon length, and colonic histopathology.

From D14 onward, the CARB/PEM, aPD-1, and combination groups exhibited slower body weight gain compared with the Model group. At D26, the Model group had significantly higher body weight than the Control group ($p < 0.05$) and all three treatment groups (all $p < 0.01$). Body weight in the combination group was lower than that in the CARB/PEM and aPD-1 groups, but the differences were not statistically significant ($p > 0.05$; Fig. 2A).

Food and water intake began to decline in all treatment groups from D14. At D24, food intake in the CARB/PEM ($p < 0.05$) and combination ($p < 0.05$) groups was significantly lower than that in the Model group; the aPD-1 group showed a non-significant decrease. No significant differences were observed among the three treatment groups (Fig. 2B). Water intake at D24 was significantly lower in the CARB/PEM ($p < 0.01$) and combination ($p < 0.01$) groups compared with the Model group; the aPD-1 group had significantly higher water intake than the CARB/PEM group ($p < 0.05$; Fig. 2C).

The spleen index, an indicator of systemic immune status, was assessed at sacrifice (D26). The Model group exhibited a significantly higher spleen index compared with the Control group ($p < 0.01$), reflecting tumor-induced splenomegaly (Fig. 2F,G). Among treatment groups, the CARB/PEM group showed a significantly lower spleen index than both the Model group ($p < 0.05$) and the aPD-1 group ($p < 0.01$). The combination group also had a significantly lower spleen index compared with the aPD-1 group ($p < 0.05$). No significant difference was observed between the CARB/PEM and combination groups, nor between the aPD-1 and Model groups. These results indicate that platinum-based chemotherapy attenuated splenomegaly, and the addition of PD-1 inhibitor did not reverse this effect.

Serum ALB and PA levels were significantly decreased in all three treatment groups compared with the Model group (all $p < 0.05$), with no significant differences among treatment groups (Fig. 2D, E).

Diarrhea symptoms began on D13–D14 in all treatment groups and progressively worsened in the CARB/PEM and combination groups. At D26, diarrhea scores in the CARB/PEM and combination groups were significantly higher than those in the Model and aPD-1 groups (all $p < 0.01$). The aPD-1 group had a slightly higher diarrhea score than the Model group, but the difference was not

significant ($p > 0.05$). No significant difference in diarrhea scores was found between the combination and CARB/PEM groups ($p > 0.05$; Fig. 3A).

DAI scores increased progressively in all groups. At D26, the Model group had significantly higher DAI than the Control group ($p < 0.05$). The CARB/PEM ($p < 0.01$) and combination ($p < 0.01$) groups had significantly higher DAI than the Model group, while the aPD-1 group did not differ from the Model group ($p > 0.05$). No significant difference was observed between the CARB/PEM and combination groups ($p > 0.05$; Fig. 3B).

Colon length was significantly shorter in the CARB/PEM ($p < 0.05$) and combination ($p < 0.05$) groups compared with the Model group. The aPD-1 group showed a slight but non-significant reduction in colon length compared with the Model group ($p > 0.05$; Fig. 3C, D).

Histopathological analysis revealed that the CARB/PEM and combination groups had significantly higher pathological scores than the Model group (9.25 ± 2.49 and 8.13 ± 2.03, respectively; both $p < 0.01$). The aPD-1 group score was not significantly different from that of the Model group ($p > 0.05$) but was significantly lower than those of the CARB/PEM and combination groups (both $p < 0.01$; Fig. 3E). HE staining showed that the Control group had intact mucosa with orderly epithelial cells, intact crypts, abundant goblet cells, and no apparent inflammatory infiltration (Fig. 3F, a). The CARB/PEM and combination groups exhibited extensive mucosal erosion, loss of crypt architecture, goblet cell depletion, and abundant lymphocyte infiltration (Fig. 3F, c, e). The aPD-1 group showed milder changes with occasional crypt distortion and mild inflammatory infiltration (Fig. 3F, d). The Model group displayed relatively normal histology with occasional epithelial shedding (Fig. 3F, b).

3.3 Intestinal barrier gene expression

At the mRNA level, both occludin and claudin-1 expression were lower in the chemotherapy and

combination groups compared with the Control, Model, and anti-PD-1 groups ($p < 0.01$ or $p < 0.05$; Fig. 3G, H). No significant difference was observed between the chemotherapy and combination groups. These results indicate that chemotherapy was associated with reduced intestinal barrier gene expression, and the addition of PD-1 inhibitor did not further alter this parameter.

3.4 Mucosal immune parameters

Foxp3 mRNA expression was significantly decreased in the CARB/PEM, aPD-1, and combination groups compared with the Control and Model groups. Foxp3 expression was lower in the aPD-1 and combination groups than in the CARB/PEM group ($p < 0.05$; Fig. 4A).

Colonic TGF-β levels in the aPD-1 and combination groups were slightly lower than in other groups, but the differences did not reach statistical significance ($p > 0.05$; Fig. 4B). No significant differences were observed among groups for colonic IL-17 levels ($p > 0.05$; Fig. 4C). Similarly, SIgA concentration and IgA+ cell ratios showed no significant differences among all five groups ($p > 0.05$; Fig. 4D, E).

In the colon, the aPD-1 group exhibited elevated IFN-γ expression at the mRNA level ($p < 0.05$) compared with the Model group, while IL-10 expression was decreased at the mRNA level ($p < 0.05$) (Fig. 5A,B). Similar changes were observed in tumor tissues: aPD-1 treatment was associated with increased IFN-γ ($p < 0.05$) and decreased IL-10 ($p < 0.05$) compared with the Model group (Fig. 5C, D).

3.5 Fecal short-chain fatty acid profile

Among the seven short-chain fatty acids quantified, only isobutyrate showed a statistically significant change among groups. Isobutyrate levels were elevated in the anti-PD-1 group compared with the Model group (23.58 ± 16.49 vs. 5.03 ± 2.30 μg/g, $p < 0.05$; Fig. 6A). The combination

group showed an intermediate level (15.67 ± 10.52 μg/g) that did not differ significantly from either the Model or the anti-PD-1 group ($p > 0.05$ for both). Acetate, propionate, butyrate, valerate, isovalerate, and hexanoate showed no significant differences among any of the five groups (all $p > 0.05$; Fig. 6B–G).

These findings indicate that PD-1 inhibitor treatment, but not chemotherapy, was associated with a selective elevation of the branched-chain short-chain fatty acid isobutyrate, in the absence of major changes in the straight-chain short-chain fatty acids.

Discussion

In this study, we descriptively characterized the intestinal toxicity profile of PD-1 inhibitor combined with platinum-based chemotherapy in an LLC mouse model. Our principal findings are: (1) combination therapy achieved superior antitumor efficacy without exacerbating GI toxicity compared with chemotherapy alone; (2) chemotherapy was associated with reduced intestinal barrier gene expression, while PD-1 inhibitor treatment was associated with changes in immune-related gene expression; and (3) PD-1 inhibitor treatment was associated with a selective elevation of the microbial metabolite isobutyrate.

The most clinically relevant finding of this study is that combining PD-1 inhibitor with platinum-based chemotherapy did not result in additive or synergistic GI toxicity, as evidenced by comparable diarrhea scores, DAI, colon shortening, and histopathological severity between the combination and chemotherapy-alone groups. This observation is consistent with clinical data showing similar rates of grade 3–4 diarrhea between combination and monotherapy regimens [7,9], and provides preclinical support for the GI safety of this widely used regimen.

Chemotherapy (both alone and in combination) was associated with reduced occludin and claudin-1 mRNA expression. The extent of barrier gene reduction was virtually identical between the chemotherapy and combination groups, indicating that chemotherapy was the primary factor associated with transcriptional changes in tight junction proteins. This is consistent with the established understanding of chemotherapy-induced intestinal mucositis, wherein DNA damage and oxidative stress lead to epithelial apoptosis and tight junction disassembly [12,13]. Barrier gene expression was assessed only at the mRNA level; whether these transcriptional changes translate to functional barrier impairment remains to be determined.

PD-1 inhibitor treatment—but not chemotherapy—was associated with changes in the mucosal immune landscape. Foxp3 mRNA, the master transcription factor of Tregs, was reduced in the aPD-1 and combination groups compared with the chemotherapy group. This is consistent with the known role of PD-1 signaling in maintaining Treg stability and suppressive function [14,19]. The concomitant elevation of IFN-γ and reduction of IL-10 in the colon, mirrored by parallel changes in the tumor microenvironment, suggests that PD-1 inhibitor treatment was associated with a systemic Th1-skewed cytokine profile. While this profile is beneficial for antitumor immunity, as reflected by the superior tumor control in our study, its relationship with intestinal mucosal changes requires further investigation.

The absence of significant changes in TGF-β, IL-17, SIgA, and IgA+ cells further refines the descriptive picture. TGF-β is a key inducer of both regulatory T cell and Th17 differentiation, yet its levels remained unchanged. Similarly, the lack of IL-17 elevation indicates that the Th17 pathway was not significantly altered in this model. Collectively, these findings suggest that the changes observed were relatively selective rather than a broad disruption of mucosal immune compartments.

The spleen index was lower in the chemotherapy and combination groups compared with the anti-PD-1 group, consistent with chemotherapy-associated myelosuppression. This systemic effect did not appear to mitigate chemotherapy-associated intestinal epithelial changes—tight junction gene reduction and mucosal damage were equally severe in the chemotherapy and combination groups. Thus, the absence of synergistic gastrointestinal toxicity in the combination group may be related to the different primary targets of the two modalities: chemotherapy primarily affecting the epithelial barrier, while PD-1 inhibitor primarily affecting the regulatory T cell–Th1 immune axis.

Our previous 16S rRNA gene sequencing analysis in this same model [18] demonstrated that chemotherapy reduced gut microbial alpha diversity, while PD-1 inhibitor treatment alone did not. The combination group did not show further diversity reduction compared with chemotherapy alone. Here we describe a functional metabolic change—the selective elevation of isobutyrate in PD-1 inhibitor-treated mice.

Isobutyrate is a branched-chain short-chain fatty acid produced by bacterial fermentation of valine [20]. Its elevation, in the absence of changes in the major straight-chain short-chain fatty acids, suggests that PD-1 inhibitor treatment was associated with altered protein or amino acid fermentation capacity of the gut microbiota rather than a global shift in carbohydrate fermentation. This is consistent with the compositional changes we reported previously [18], which showed selective alterations in specific bacterial taxa rather than global shifts in community structure. The functional significance of elevated isobutyrate remains to be determined; whether it acts as a

bystander metabolite reflecting microbiota changes or contributes to the observed immune and barrier changes warrants further investigation through interventional studies.

Several limitations of this study should be acknowledged. First, intestinal barrier and immune parameters were assessed primarily at the mRNA level; protein-level validation by Western blot was not performed. Second, regulatory T cell numbers and function were not directly assessed by flow cytometry. Third, the functional significance of elevated isobutyrate was not validated through intervention experiments. Fourth, the sample size (n = 8 per group) may limit statistical power for detecting subtle differences. Fifth, the follow-up period of 14 days may not capture delayed or chronic intestinal toxicity. Finally, causal relationships between the observed immune, barrier, and metabolic changes cannot be established from this descriptive study. Future studies incorporating protein-level validation, functional immune assays, and interventional approaches are warranted.

In conclusion, this descriptive study shows that PD-1 inhibitor combined with platinum-based chemotherapy achieved maximal antitumor efficacy without synergistic gastrointestinal toxicity in a Lewis lung carcinoma mouse model. Chemotherapy was associated with reduced intestinal barrier gene expression, while PD-1 inhibitor treatment was associated with changes in immune-related gene expression and a selective increase in the microbial metabolite isobutyrate. These observations suggest associations that warrant further investigation to establish causal relationships.

Conflict of Interest

The authors declare that the research was conducted in the absence of any commercial or financial relationships that could be construed as a potential conflict of interest.

Ethical statement: This study was approved by The Animal Care and Use committee of Qilu Hospital of Shandong University（No.KYLL-2022(ZM)-1121）

Funding: This study has received funding by Grants ZR2023QH485 and ZR2023QH328 from Natural Science Foundation Committee of Shandong Province.

Data availability: The data that support the findings of this study are openly available in GSA repository at https://ngdc.cncb.ac.cn/gsa/s/8z42ieyP, reference number [CRA045001]. Shared URL: https://ngdc.cncb.ac.cn/gsa/s/61jWwApT

References

[1] Reck M, et al. Pembrolizumab versus chemotherapy for PD-L1-positive non-small-cell lung cancer. N Engl J Med. 2016;375:1823--1833.

[2] Gandhi L, et al. Pembrolizumab plus chemotherapy in metastatic non-small-cell lung cancer. N Engl J Med. 2018;378:2078--2092.

[3] Paz-Ares L, et al. Pembrolizumab plus chemotherapy for squamous non-small-cell lung cancer. N Engl J Med. 2018;379:2040--2051.

[4] Gadgeel S, et al. Updated analysis from KEYNOTE-189: pembrolizumab or placebo plus pemetrexed and platinum for previously untreated metastatic nonsquamous non-small-cell lung cancer. J Clin Oncol. 2020;38:1505--1517.

[5] Postow MA, et al. Immune-related adverse events associated with immune checkpoint blockade. N Engl J Med. 2018;378:158--168.

[6] Soularue E, et al. Enterocolitis due to immune checkpoint inhibitors: a systematic review. Gut. 2018;67:2056--2067.

[7] Langer CJ, et al. Carboplatin and pemetrexed with or without pembrolizumab for advanced,

non-squamous non-small-cell lung cancer: a randomised, phase 2 cohort of the open-label KEYNOTE-021 study. Lancet Oncol. 2016;17:1497--1508.

[8] Rizvi NA, et al. Nivolumab in combination with platinum-based doublet chemotherapy for first-line treatment of advanced non-small-cell lung cancer. J Clin Oncol. 2016;34:2969--2979.

[9] Herbst RS, et al. Pembrolizumab versus docetaxel for previously treated, PD-L1-positive, advanced non-small-cell lung cancer (KEYNOTE-010): a randomised controlled trial. Lancet. 2016;387:1540--1550.

[10] Peterson LW, Artis D. Intestinal epithelial cells: regulators of barrier function and immune homeostasis. Nat Rev Immunol. 2014;14:141--153.

[11] Kayama H, et al. Interaction between the microbiota, epithelia, and immune cells in the intestine. Annu Rev Immunol. 2020;38:23--49.

[12] Sonis ST. The pathobiology of mucositis. Nat Rev Cancer. 2004;4:277--284.

[13] Wardill HR, Bowen JM. Chemotherapy-induced mucosal barrier dysfunction: an updated review on the role of intestinal tight junctions. Curr Opin Support Palliat Care. 2013;7:155--161.

[14] Luoma AM, et al. Molecular pathways of colon inflammation induced by cancer immunotherapy. Cell. 2020;182:655--671.

[15] Coutzac C, et al. Colon immune-related adverse events: anti-CTLA-4 and anti-PD-1 blockade induce distinct immunopathological entities. J Crohns Colitis. 2017;11:1238--1246.

[16] Arpaia N, et al. Metabolites produced by commensal bacteria promote peripheral regulatory T-cell generation. Nature. 2013;504:451--455.

[17] Furusawa Y, et al. Commensal microbe-derived butyrate induces the differentiation of colonic regulatory T cells. Nature. 2013;504:446--450.

[18] Dai L, Kong F-L. Effect of programmed cell death protein-1 inhibitor combined with platinum-containing dual-agent chemotherapy regimen on gut microbiota in Lewis lung cancer model mice. Front Microbiol. 2026;17:1885048.

[19] Francisco LM, et al. PD-L1 regulates the development, maintenance, and function of induced regulatory T cells. J Exp Med. 2009;206:3015--3029.

[20] Macfarlane GT, Macfarlane S. Bacteria, colonic fermentation, and gastrointestinal health. J AOAC Int. 2012;95:50--60.

Figure Legends

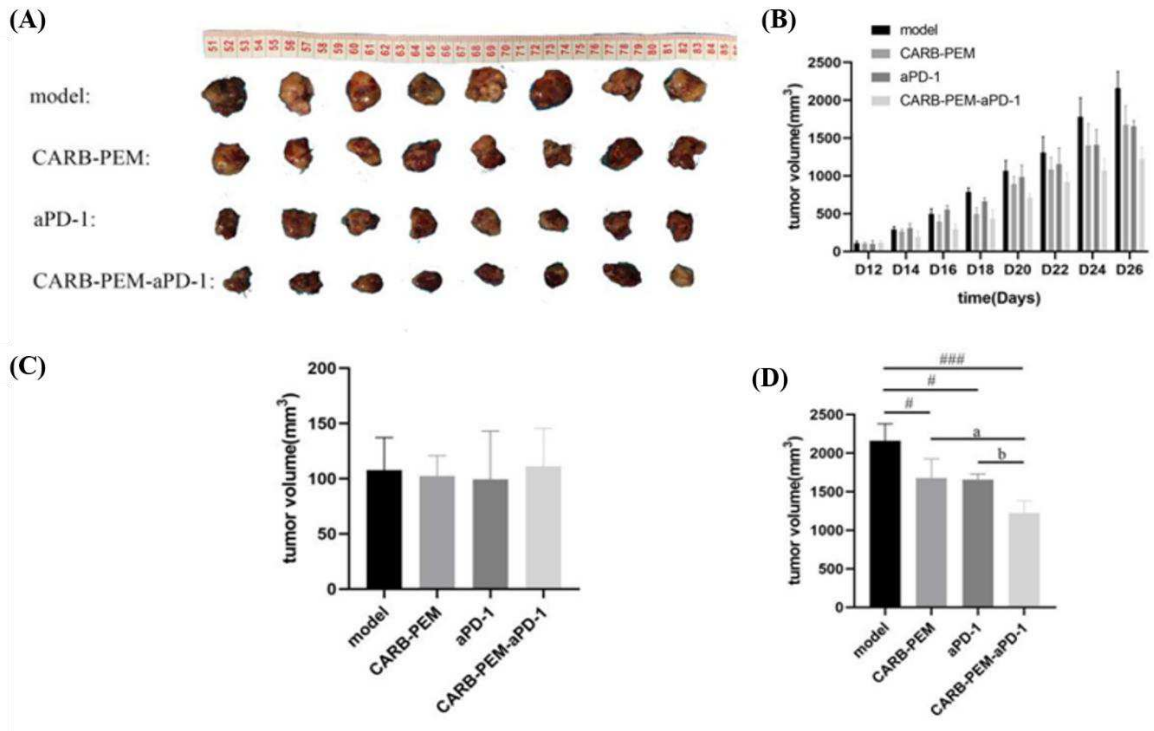


Figure 1. Antitumor efficacy of combination therapy. (A) Representative gross images of excised tumors at D26. (B) Tumor volumes of LLC-bearing mice in the Model, CARB/PEM, aPD-

1, and combination groups. (C) Comparison of tumor volumes between Model, CARB/PEM, aPD-1, and combination groups. (D) Final tumor volumes at D26. Data are presented as mean ± SD (n=8). *p < 0.05, **p < 0.01 vs. Model; #p < 0.05 vs. CARB/PEM group and aPD-1 group.

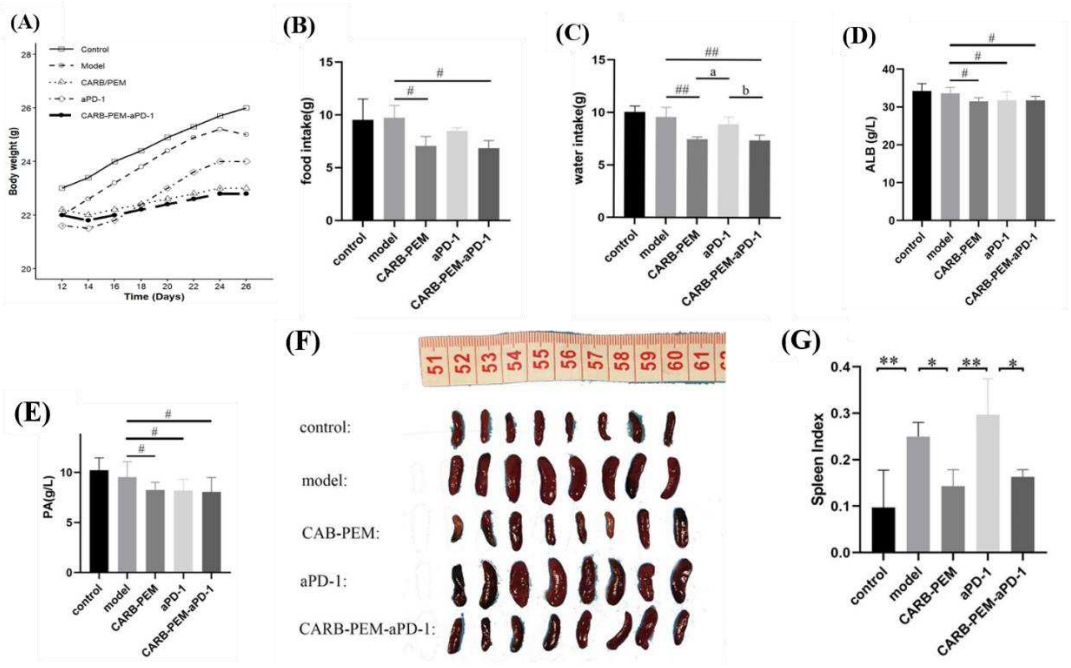


Figure 2. Effects of treatments on general condition and nutritional status. (A) Body weight change curves. (B) Food intake at D24. (C) Water intake at D24. (D) Serum albumin (ALB) levels. (E) Serum prealbumin (PA) levels. (F, G) Spleen index. Data are presented as mean ± SD (n=8). *p < 0.05, **p < 0.01.

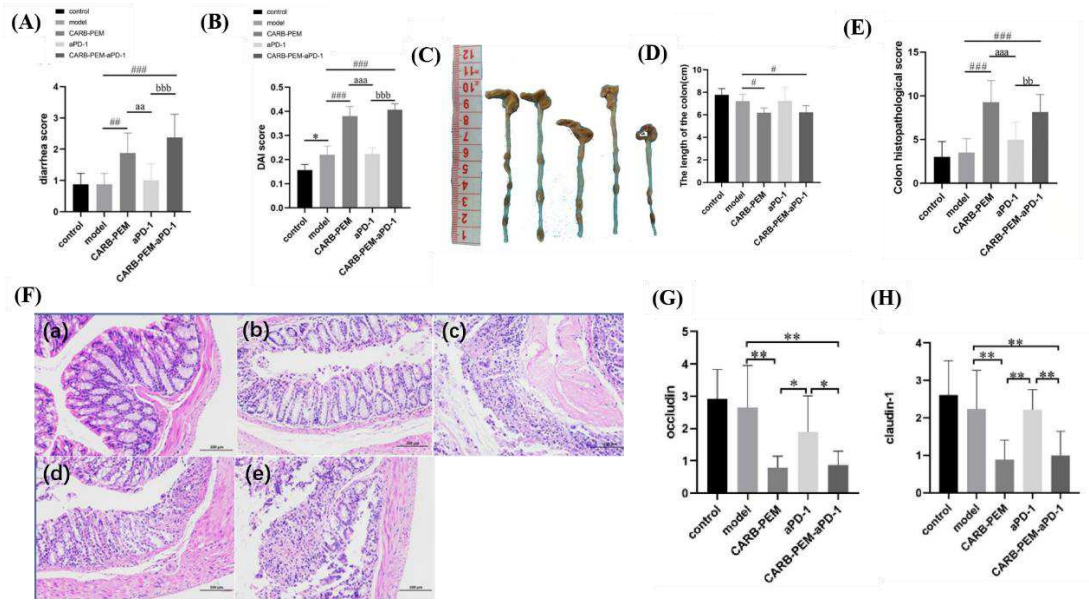


Figure 3. Gastrointestinal toxicity and intestinal barrier integrity in LLC-bearing mice. (A) Diarrhea scores at D26. (B) Disease activity index (DAI) scores at D26. (C) Representative images of colons. (D) Colon length measurements. (E) Histopathological scores. (F) Representative HE-stained colon sections (100× magnification): (a) Control, (b) Model, (c) CARB/PEM, (d) aPD-1, (e) Combination. Scale bar = 100 μm. (G) Relative mRNA expression of occludin in colon tissues. (H) Relative mRNA expression of claudin-1 in colon tissues. Data are presented as mean ± SD (n=8). *p < 0.05, **p < 0.01. For panels G and H, significance refers to comparisons between CARB/PEM or combination groups versus Control, Model, or aPD-1 groups. CARB/PEM, carboplatin/pemetrexed; aPD-1, anti-PD-1 antibody; DAI, disease activity index; HE, hematoxylin-eosin.

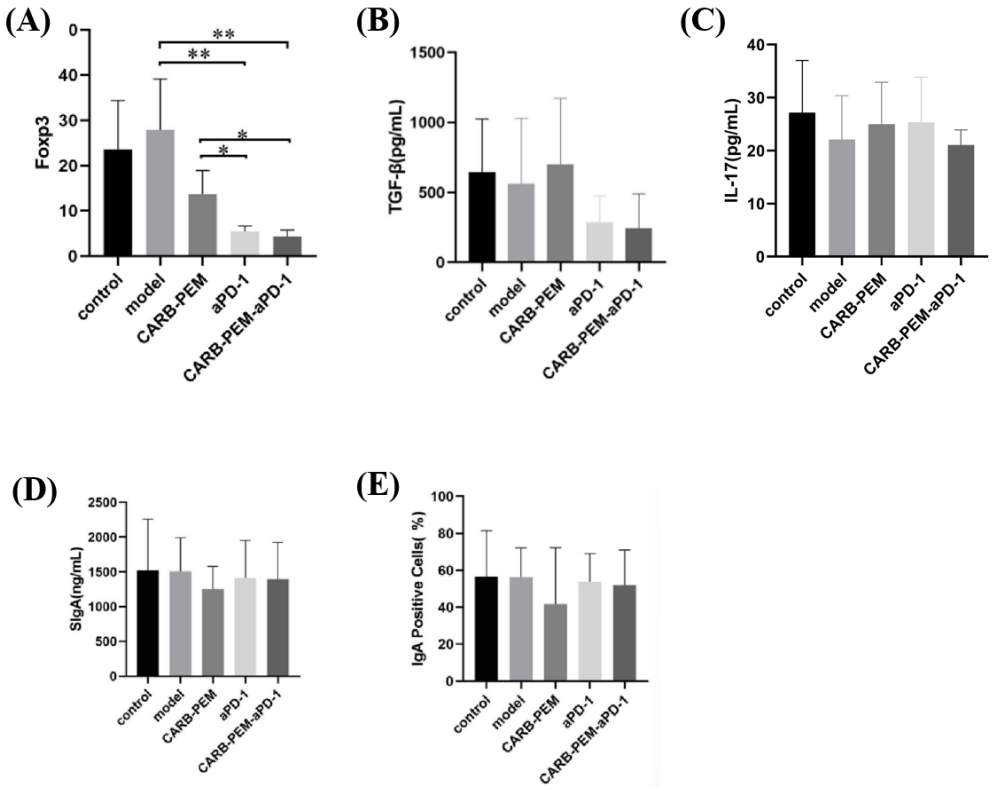


Figure 4. Mucosal immune parameters. (A) Foxp3 mRNA expression in colon tissues. (B) Colonic TGF-β levels. (C) Colonic IL-17 levels. (D) Colonic SIgA concentration. (E) IgA+ cell ratios in colonic mucosa. Data are presented as mean ± SD (n=8). *p < 0.05, **p < 0.01.

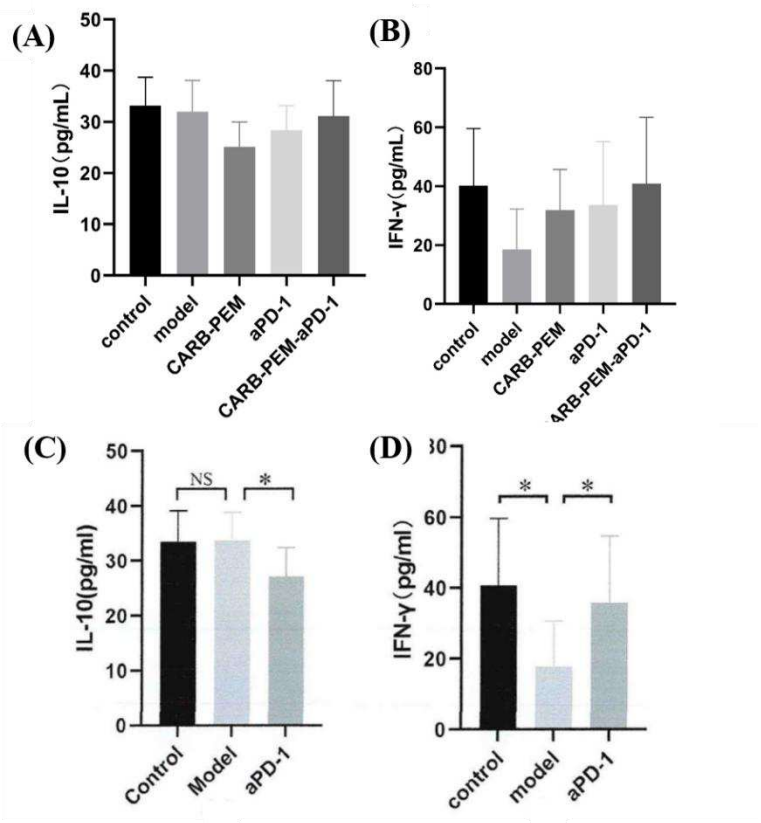


Figure 5. Inflammatory cytokine expression in colon and tumor tissues.

(A) Colonic IL-10 mRNA expression (n=8 per group).(B) Colonic IFN-γ mRNA expression (n=8 per group). (C) Tumor IL-10 levels measured by ELISA (n=8 per group).(D) Tumor IFN-γ levels measured by ELISA (n=8 per group). Data are presented as mean ± SD. *p < 0.05, **p < 0.01 vs. Control group; #p < 0.05, ##p < 0.01 vs. Model group.

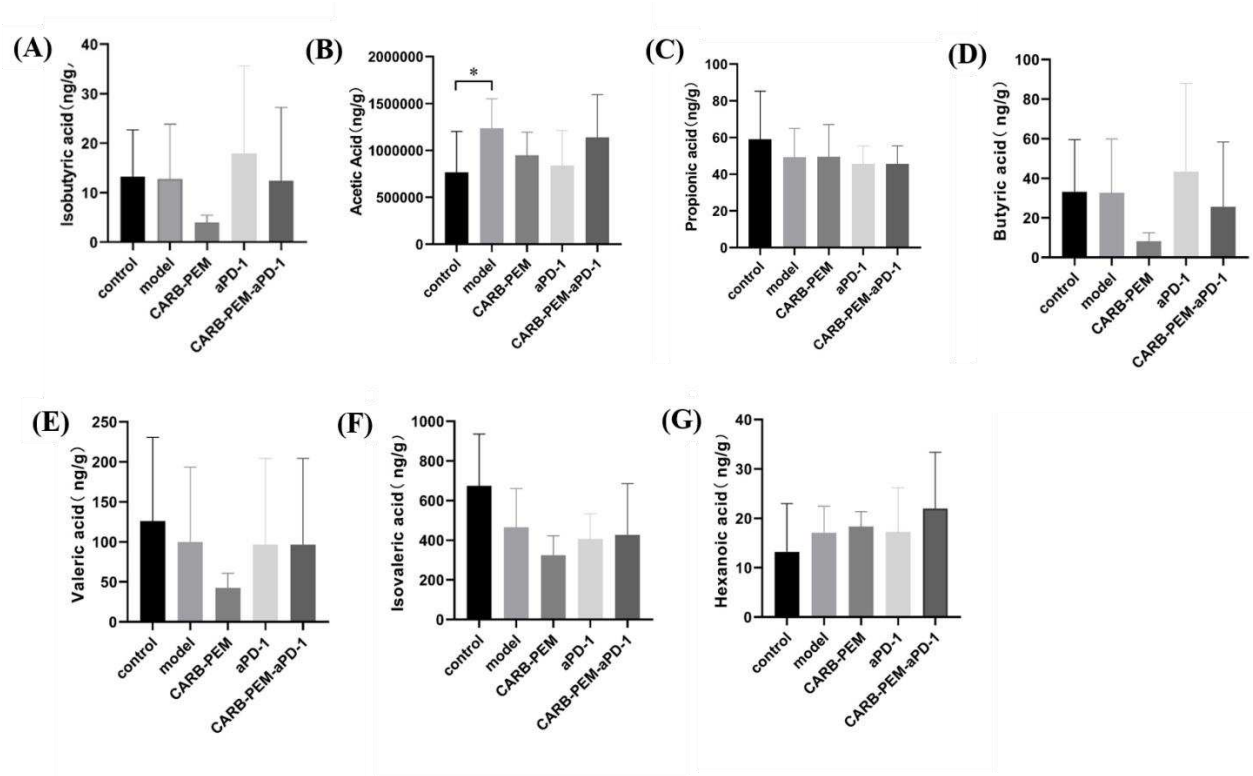


Figure 6. Fecal short-chain fatty acid (SCFA) profiles. Targeted LC-MS/MS quantification of seven SCFAs in fecal samples collected at D26: (A) isobutyrate, (B) acetate, (C) propionate, (D) butyrate, (E) valerate, (F) isovalerate, (G) hexanoate. Data are presented as mean ± SD (n=8). *p < 0.05 by Kruskal-Wallis test followed by Dunn's post-hoc test. Only isobutyrate showed a statistically significant difference among groups, with elevated levels in the aPD-1 group compared with the Model group.